1997

Reflection High-Energy Electron-Diffraction Study of Melting and Solidification of Pb on Graphite

Z. H. Zhang
Old Dominion University

P. Kulatunga
Old Dominion University

H. E. Elsayed-Ali
Old Dominion University, helsayed@odu.edu

Original Publication Citation

Zhang, Z. H., Kulatunga, P., & Elsayed-Ali, H. E. (1997). Reflection high-energy electron-diffraction study of melting and solidification of Pb on graphite. *Physical Review B, 56*(7), 4141-4148. doi:10.1103/PhysRevB.56.4141

Reflection high-energy electron-diffraction study of melting and solidification of Pb on graphite

Z. H. Zhang
Department of Electrical and Computer Engineering, Old Dominion University, Norfolk, Virginia 23529

P. Kulatunga
Department of Physics, Old Dominion University, Norfolk, Virginia 23529

H. E. Elsayed-Ali*
Department of Electrical and Computer Engineering, Old Dominion University, Norfolk, Virginia 23529
(Received 24 June 1996; revised manuscript received 20 February 1997)

The melting and solidification of Pb thin films on pyrolytic graphite are investigated *in situ* by reflection high-energy electron diffraction. Thin films with thicknesses of 4–150 monolayers are investigated. The surface morphology of the thin films were studied by scanning electron microscopy. Superheating of the Pb thin films by 4 ± 2 to 12 ± 2 K is observed from diffraction intensity measurements. Upon cooling the substrate, the Pb on graphite is seen to supercool by $\sim 69\pm4$ K. [S0163-1829(97)05431-3]

I. INTRODUCTION

Superheating of micrometer-sized Pb crystallites bounded by close-packed facets grown on graphite, by a few degrees above the Pb bulk melting point, $T_m = 600.7$ K, has been previously observed.[1–3] Métois and Heyraud were able to produce a large number of polyhedral Pb crystallites on graphite in an ultrahigh vacuum scanning electron microscope (UHV-SEM). Of these, the sharp edged Pb crystallites with extensive {111} facets were seen to superheat by 3 K. The formation of {111} facets near the melting point were confirmed by SEM studies.[1,4] Spiller observed superheating of irregularly shaped Pb microcrystallites by 2 K. These were obtained by depositing 5- and 50-Å thick films of Pb onto a graphite substrate at 470 K.[2] The sample was prepared in a low vacuum (10^{-7} Torr) and observed *in situ* using SEM. Recent theoretical calculations predicted that surface superheating is related to the partial wetting angle of the surface, and the tilt angle of the melted regions in a vicinal surface undergoing nonmelting induced faceting.[5] Superheating of coated clusters has also been theoretically investigated. These simulations show that the degree of superheating depends on coating thickness.[6] In 180-ps pulsed laser heating of Pb(111), superheating by 120 K was observed in time-resolved reflection high-energy electron-diffraction (RHEED) experiments.[7–9] Much less superheating was also observed in pulsed laser heating experiments of Pb(100).[10]

We report on the melting and solidification characteristics of thin films of Pb on graphite using *in situ* RHEED. Pb films with thicknesses ranging from a few monolayers (ML) to 150 ML are studied. The surface Debye temperature is calculated from the temperature-dependent RHEED intensity. For the investigated film thicknesses, epitaxial growth of Pb at room temperature may occur in a layer-by-layer growth mode. Multilayers of Pb grown on graphite offer a relatively simple two-dimensional (2D) system to study the melting and solidification of thin films. The interaction of Pb with the graphite is purely through van der Waals forces, and complications due to chemical reactions are not present. In the present study, we observed the melting and solidification of Pb films of thicknesses 4, 14, 70, and 150 ML on graphite. Surface morphology was observed by SEM. Superheating by $4-(12\pm2)$ K above the bulk melting temperature, and supercooling of the Pb by 69 ± 4 K were observed.

II. EXPERIMENTAL METHOD

An ultrahigh vacuum chamber equipped with a RHEED system was used in this study. The residual gas pressure in the chamber was less than 5×10^{-10} Torr except during Pb deposition, at which time the vacuum was $\sim 6\times10^{-9}$ Torr. The electron-beam energies used were 12 and 15 keV. A $12\times12\times2$ mm^3 pyrolytic graphite (0002) substrate was used. A clear RHEED pattern of the graphite surface was obtained by peeling off a few layers immediately prior to loading the sample in the UHV chamber. Further cleaning of the substrate was not necessary due to the inertness of the graphite surface; however, the sample was heated at 450 °C for 6 h prior to Pb deposition. Pb was deposited on the graphite substrate using a molybdenum basket, and the deposition rate was monitored with a quartz-crystal thickness monitor. The deposition rates varied from 12 Å/min for the 4-ML films, to 240 Å min for the 150-ML films. The higher deposition rate for the thicker film was to minimize the possibility of contamination during deposition. Pb deposited on the graphite can be evaporated by heating the sample for several minutes at 600 °C. This was verified by the clear RHEED pattern of the graphite surface.

The substrate was mounted on a resistively heated stage capable of reaching temperatures up to 1000 °C. The temperature was measured by a *K*-type thermocouple which was clipped onto the substrate surface. The thermocouple was calibrated to the bulk melting temperature of Pb, and the boiling point of distilled water. These results showed an uncertainty of ±2 K near the Pb melting point and ±1 K near the boiling point of water.

RHEED peak intensity measurements are carried out by an imaging system with a charge-coupled detector (CCD)

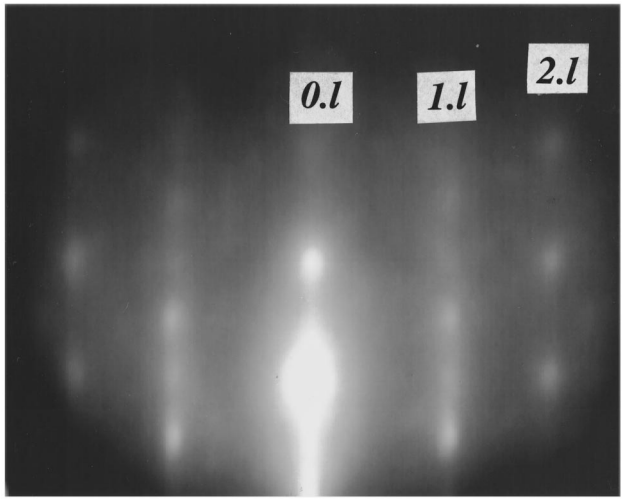

FIG. 1. A RHEED pattern taken of the clean graphite (0002) surface with a 12-keV electron-beam incident along the [110] direction. The angle of incidence of the electron beam was ~3 corresponding to the Bragg condition of the graphite surface.

interfaced to a personal computer. Several of the Pb films were removed from the UHV chamber for SEM observations. The Pb growth mode and crystal shape were investigated.

The graphite substrate used in the present experiment is a commercial pyrolytic monochromator type.[11,12] Since naturally occurring graphite single crystals are relatively small and difficult to obtain, the most widely studied form of graphite are these highly orientated pyrolytic graphite. This polycrystalline material with a hexagonal structure has a grain size of about 3–10 μm, and a good c^*-axis orientation (misorientation angle less than 2°).[13–17]

III. RESULTS

Figure 1 is a RHEED pattern taken of the clean graphite (0002) surface with a 12-keV electron beam incident along the [110] direction. The incident angle of the electron beam was ~3°, corresponding to the Bragg condition of the graphite surface. In the pattern, the three-dimensional diffraction spots of graphite can be clearly observed. The broad spots are arranged in a rod along the vertical direction in the order 0.l, 1.l, 2.l with periodically varying intensities along the direction perpendicular to the surface. The 0.l and 1.l rods are brighter than the 2.l rod, particularly the specular beam which shows the maximum intensity.

We calculate the reciprocal-lattice structure of graphite using the atom positions (0,0,0), $(0,0,\frac{1}{2})$, $(\frac{1}{3},\frac{2}{3},\frac{1}{2})$, and $(\frac{2}{3},\frac{1}{3},0)$ of the Bravais unit cell. The reciprocal spot intensity is given by

$$J_{hkl}=f^2[1+\cos\pi l+\cos\pi(\tfrac{4}{3}h+\tfrac{2}{3}k)+\cos\pi(\tfrac{2}{3}h+\tfrac{4}{3}k+l)]^2+f^2[\sin\pi l+\sin\pi(\tfrac{4}{3}h+\tfrac{2}{3}k)+\sin\pi(\tfrac{2}{3}h+\tfrac{4}{3}k+l)]^2,$$

where h, k, and l are the Miller indices. Thus, the diffraction spots (001), (003), (111), (333), (310), and (121) disappear

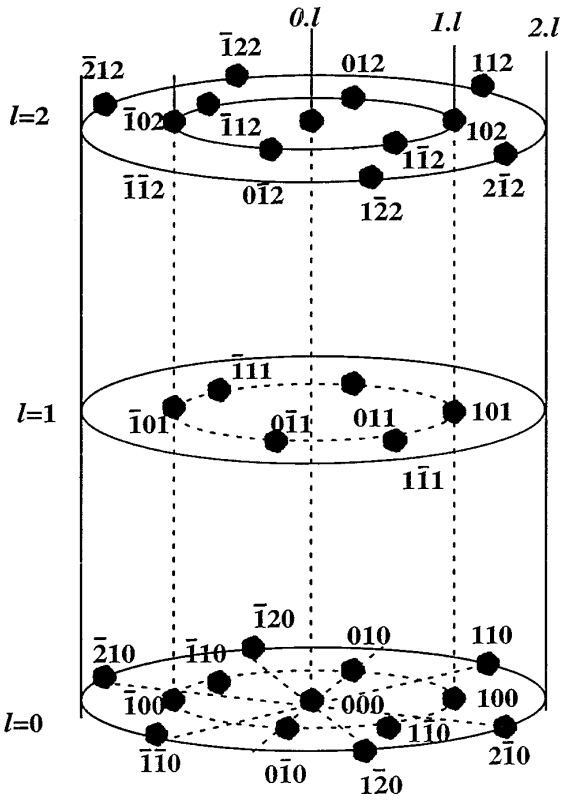

FIG. 2. The reciprocal-lattice structure of graphite. The 0.l, 1.l, and 2.l rods are shown intersecting the Ewald sphere (approximated by the plane of the paper).

due to the prohibition principle. Figure 2 shows the reciprocal-lattice structure in which 0.l, 1.l, and 2.l rods intersect the Ewald sphere that corresponds to the same rods in the RHEED pattern as shown in Fig. 1. For [110] incidence, it is clear from the reciprocal lattice that the 0.l and 1.l lines intersect the reciprocal spots as shown by the concentric solid circles. The 2.l line does not intersect any of the spots, but in the pattern the 2.l rod can be clearly seen along with the 0.l and 1.l rods. When the crystal is rotated about the [001] axis, the rods remain observable in all azimuthal orientations, but their intensities change with the azimuthal angle. As shown in Fig. 1, when the electron beam is incident along the [110] direction, the 0.l and 1.l rods are relatively strong. The intensity of the 1.l ($l=0$) rod is maximum. However, when the crystal is turned 60° parallel to [010] direction, the 1.l rod remains visible, but with low intensity. This shows that the reciprocal lattice of the pyrolytic graphite is rotated about the c^* axis to produced smeared out rings of the reciprocal-lattice points except along the c^*-axis direction. The surface of the graphite substrate consists of a collection of small crystals. These crystals have a c^*-axis texture structure. Even though the crystals are randomly oriented, there is a preferred crystal orientation. From the separation width between the 0.l and 1.l rods, the measured lattice constant is 4.24 Å. This corresponds to the diagonal distance of 4.25 Å corresponding to the graphite unit cell in the [110] direction, whereas the in-plane lattice-constant is 2.46 Å.

The incident angle of the electron beam was varied to trace the 002, 004, and 006 Bragg reflection spots. The corresponding incident angles were measured. The inner poten-

TABLE I. Angle of incidence at Bragg condition for graphite.

	n	1	2	3	4	5	6
15 keV	θ		0.48	1.97	2.98	3.94	4.85
12 keV	θ		0.54	2.21	3.36	4.42	5.45

TABLE II. Angle of incidence at Bragg condition for Pb.

	n	1	2	3	4	5	6
15 keV	θ		0.86	2.40	3.57	4.68	5.74
12 keV	θ		0.96	2.68	4.00	5.24	6.43

tial V_0 of the graphite (0002) surface was calculated using the expression $V_0 = E(\sin\theta^2 - \sin\theta_0^2)$.[18] Here $\sin\theta_0$ is given by the Bragg condition as $2d\sin\theta_0 = n\lambda$, where d is the interplanar distance perpendicular to the graphite (0002) surface, which is given by 3.35 Å. V_0 thus obtained is 12.3 eV. The angles of incidence satisfying the Bragg condition calculated using this value for a few of the diffraction spots at $E = 15$ keV, and $E = 12$ keV are given in Table I.

Pb was deposited onto the clean graphite surface as described previously. Figure 3 shows a RHEED pattern after the deposition of approximately 4 ML of Pb. The 12-keV beam incident along the [110] direction of the graphite crystal. In the RHEED pattern, spots and rods (streaks) can be seen. The diffraction spots along the 0.l rod, and particularly the specular beam, are seen to be sharper for Pb than for the graphite pattern shown in Fig. 1. The Pb.l rod is seen between the 0.l and the 1.l rods of graphite. The measured lattice distance obtained from the separation between the Pb.l and the 0.l rod is 5.72 Å, in reasonable agreement with 6.06 Å diagonal length of the Pb(111) unit cell in the [100] direction. The difference could be attributed to the inaccuracy in the RHEED measurement due to the diffuse nature of the Pb spots. Similar to the graphite surface, when the crystal was rotated, each Pb rod remains visible in the pattern, indicating that the reciprocal lattice is circularly rotated about the [111] axis of Pb. The intensities also change with the azimuthal angle and has its maximum when the Pb[100] direction is parallel to the graphite [110] direction. This indicates that the Pb crystallites have a texture structure, similar to the graphite substrate, such that the Pb crystallites are rotated about the [111] axis with respect to each other. Therefore, we conclude that Pb grows in layers oriented with Pb{111} parallel to {0002} of graphite, $(111)_{\mathrm{Pb}} \| (0002)_{\mathrm{graphite}}$, and $[100]_{\mathrm{Pb}} \| [\bar{1}10]_{\mathrm{graphite}}$. By using 14.9 eV for the inner potential of Pb, the incident angles correspond to the Bragg condition are given in Table II.[19]

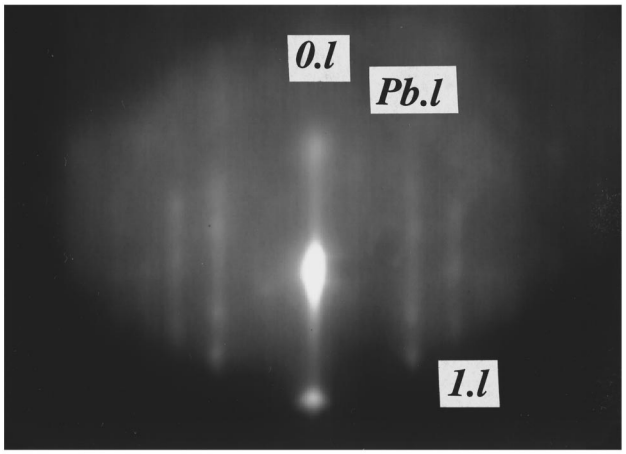

FIG. 3. A RHEED pattern after the deposition of approximately 4 ML of Pb.

For a 12-keV electron energy, the Bragg condition corresponding to $n = 3$ for graphite and Pb, is calculated to be 2.21° and 2.68° respectively. This indicates that the Bragg reflection spots are separated on the RHEED screen, in a direction perpendicular to the sample. Therefore, measurement of the Pb spot intensity is not affected by the graphite spot intensity. The specular beam from the 4-ML Pb film was analyzed in order to investigate the temperature dependence of the spot intensity. The specular beam intensity is strong enough to remain visible up to the melting point, and its shape and intensity contain information on crystallite size and any phase change of the deposited Pb layers. The intensity change of the specular beam is the least affected by increasing temperature during Pb film heating up to its melting point. Higher-order diffracted beams from the Pb film become increasingly weak as the temperature is raised. Figure 4(a) shows the intensity of the (333) Bragg reflection spot of Pb at an electron incidence angle of 2.57° (near 2.68° corresponding to the calculated Bragg condition), as a function of the substrate temperature. The small difference between the angles of incidence corresponding to $n = 3$ Bragg condition and the calculated angle in Table II is within the experimental error, or might be due to dynamical effects. The two curves corresponding to heating and cooling are distinguished by two arrows in opposite directions. The temperature was raised from 343 to 633 K, in about 10 min at an approximately constant rate of 0.5 deg. After reaching the maximum desired temperature, the power to the heater is turned off and the substrate is allowed to cool in a vacuum. The substrate cools to ~373 K in about 30 min. Figure 4(b) shows the intensity change at the higher temperature range extracted from Fig. 4(a). The abrupt change in the diffraction spot intensity upon heating and cooling is due to melting and solidification, respectively. In the temperature range between 601 and 606 K, the intensity drops abruptly. Above 606 K the intensity remains almost unchanged. The drop in intensity begins at 601 K, about the same as the bulk melting point of Pb ($T_m = 600.7$ K), but remains above the constant intensity level that is reached at 606 K as seen in Fig. 4(b). This indicates partial melting of the Pb thin film at the bulk melting point, $T_m = 600.7$ K, while some of the Pb crystallites superheat, remaining solid at and above T_m. During cooling, the intensity undergoes a large change over the temperature range 535 to 530 K, a much lower temperature than the melting point. As the temperature falls below 530 K, the intensity increases exponentially indicating supercooling of the Pb film. The Pb rods, except the (00) rod, became too weak to observe about 570 K during heating, and reappeared about 530 K during cooling. We did not observe any additional diffraction spots except for those that were confirmed to be from Pb{111} during heating. This means that only

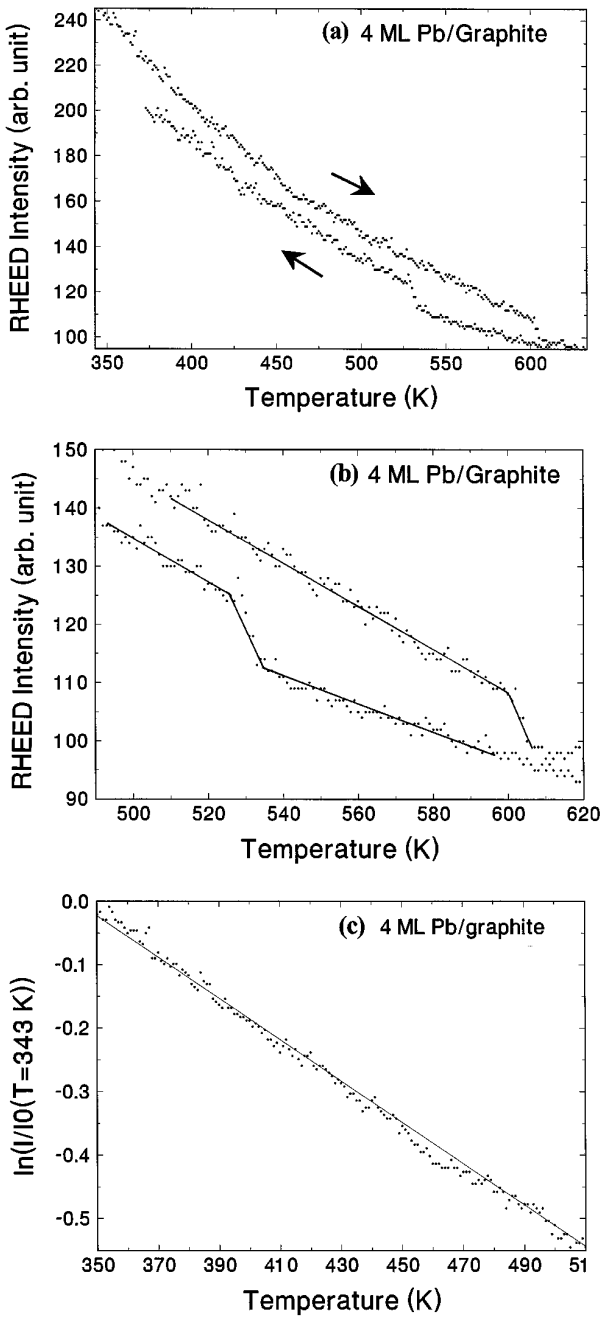

FIG. 4. (a) The intensity of the (333) Bragg reflection spot of 4-ML Pb for an incidence angle of 2.57, as a function of the substrate temperature. The two curves corresponding to heating and cooling are distinguished by two arrows in opposite directions. The temperature was raised from 343 to 633 K, and then lowered to 373 K. (b) The intensity change at the higher temperature-range extracted from (a), showing an abrupt change in the diffraction spot intensity due to the melting and solidification phase transitions. (c) The semi-logarithmic of RHEED intensity at temperatures lower than 493 K during heating is plotted. The Debye-Waller factor is obtained from a least-squares-fit to this curve. The Debye temperature obtained is 79 ± 3 K.

crystallites with the Pb(111) orientation are formed during heating. As the temperature was increased from room temperature to 590 K, the intensity decreased exponentially, as shown in Fig. 4(a). The logarithm of the normalized RHEED intensity at temperatures lower than 493 K during heating is

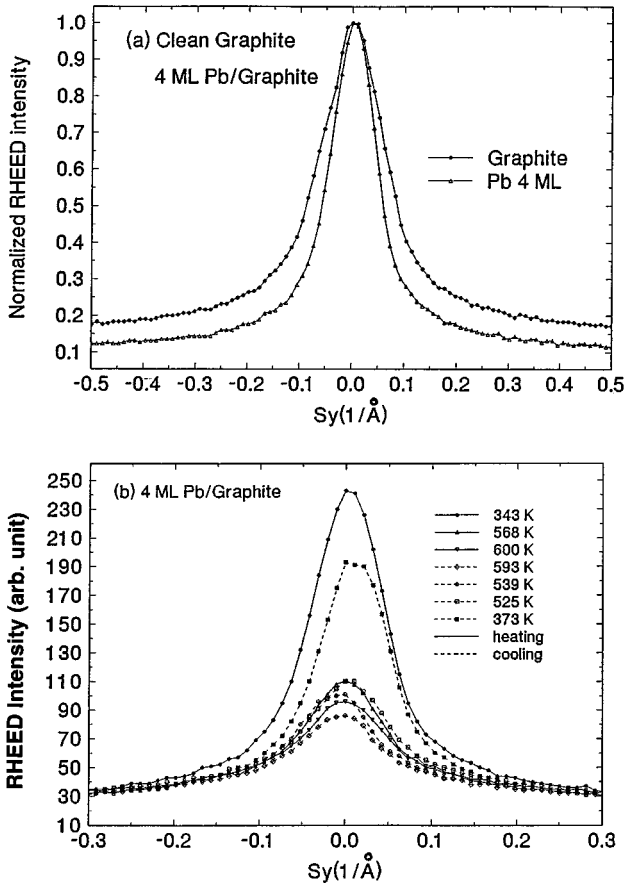

FIG. 5. (a) RHEED intensity profiles of the clean graphite surface, and the 4 ML of Pb deposited graphite surface. The estimated average sizes of the graphite and deposited crystallites of Pb are 106 ± 53 and 230 ± 115 Å. (b) The changes of the RHEED intensity profile of 4-ML Pb during heating and cooling.

plotted in Fig. 4(c). The Debye-Waller factor is obtained from a least-squares fit to this curve. The Debye temperature thus calculated is 79 ± 3 K, which is higher than the surface Debye temperature of 66 K for Pb(111), and lower than 88 K of bulk Pb.[20]

The peak profile of the specular beam was analyzed. Figure 5(a) shows the RHEED intensity profiles taken of the clean graphite surface and of the surface of the 4-ML thick Pb film at the in-phase condition. Spots in the RHEED pattern are due to the transmission of the electron beam through the three-dimensional small crystallites on the substrate. Therefore, the full width at half maximum (FWHM) of the intensity profile of such spots depends upon the average crystallite size. The intensity profile of both the lead and graphite RHEED spots in the in-phase condition shows a good fit to a Lorentzian profile. The FWHM of the peak intensity profile of the Pb spot is seen to be smaller than that of the graphite. The measured FWHM full width at half maximum is 0.118 and 0.150 Å^{-1} for the graphite substrate and for the 4-ML Pb film, respectively. The instrumental response is determined from the FWHM of the direct beam on the screen. Then the average size of the graphite and the Pb crystallites is calculated using the following expression: $2\pi/(\text{FWHM}-\text{instrumental response})$. Taking into account an instrumental response of 0.091 Å^{-1}, the average graphite and Pb crystallite size is found to be 106 ± 53 Å and 230

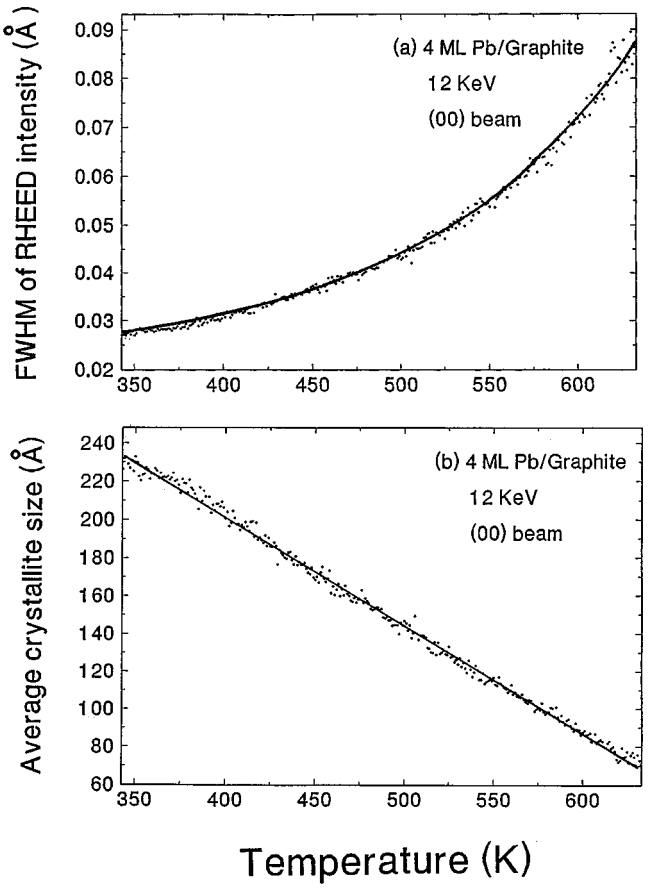

FIG. 6. (a) Change of FWHM by fitting to a Lorentzian during heating. The FWHM changes from 0.027 to 0.090 $Å^{-1}$. (b) The measured average crystallite size with temperature. The average crystallite size changes from 230 ± 115 to 70 ± 35 Å.

± 115 Å, respectively, indicating that the Pb crystallites are larger than the graphite. Figure 5(b) shows RHEED intensity profiles of 4 ML of Pb on graphite during heating and cooling. The peak intensity decreases with temperature and the FWHM becomes larger. This indicates that the average size of the crystallites decreases as the temperature approaches T_m. When the sample is cooled the intensity increases and the FWHM becomes smaller. This shows that the crystallites growing from the supercooled melt increase in size as the temperature drops. Figure 6(a) shows the change in FWHM of the peak profile during heating. The FWHM increases from 0.027 to 0.090 $Å^{-1}$. After taking the instrumental response into account, the calculated average crystallite size is shown in Fig. 6(b) as a function of temperature. The average crystallite size changes from 230 ± 115 to 70 ± 35 Å, with the size decreasing to less than 100 Å near the melting point. This indicates that melting is preceded by the formation of small crystallites.

In the case of the 14 ML of Pb on graphite, the Pb RHEED spot intensity is brighter than those observed for 4-ML Pb. The graphite spots, however, are not as visible in this case as for the 4-ML case. This indicates that the Pb layer on the graphite nearly covers the whole graphite surface with {111} oriented Pb. The sample was heated to 633 K, then cooled to 423 K, and the Pb RHEED spot intensity measurement was repeated. Figures 7(a) and 7(b) show

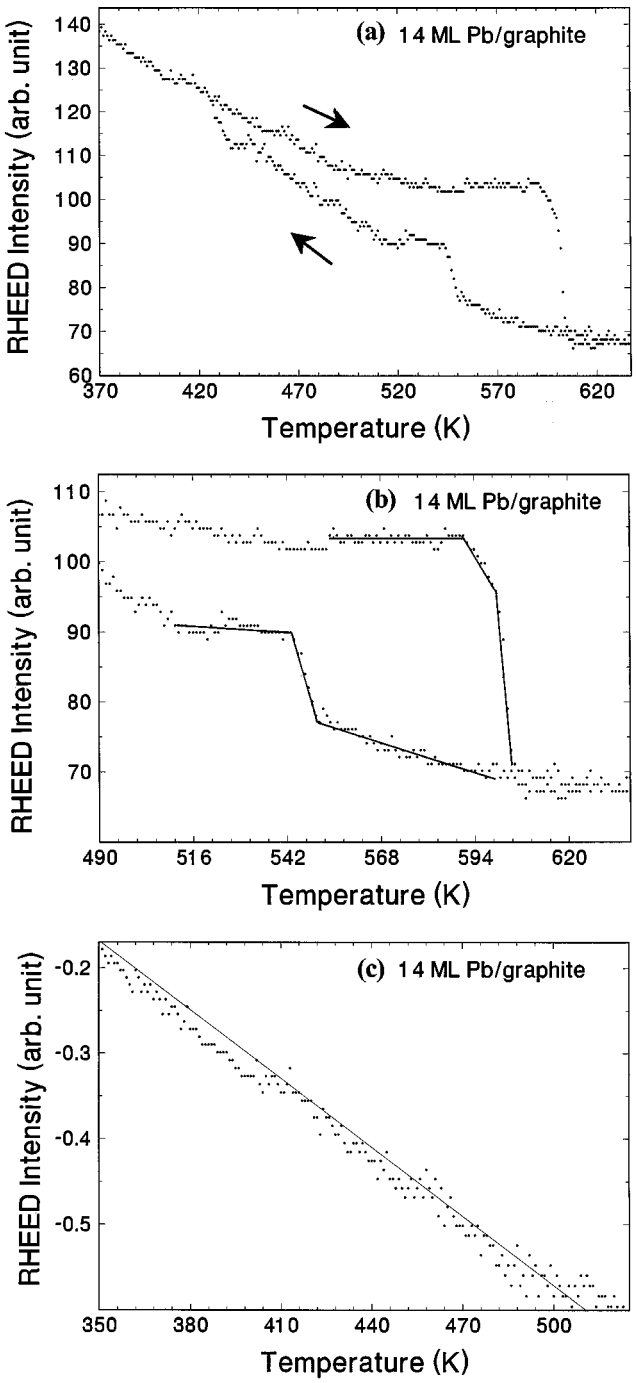

FIG. 7. (a) The intensity of the (333) Bragg reflection spot of the 14-ML Pb as a function of temperature. The two curves corresponding to heating and cooling are distinguished by two arrows in opposite directions. The temperature was raised from 343 to 633 K, and then lowered to 373 K. (b) The intensity change at the higher temperature-range extracted from (a) showing an abrupt change in the diffraction spot intensity due to melting and solidification. (c) A semilogarithmic plot of RHEED intensity as a function of temperature during heating. A Debye temperature of 91 ± 3 K is obtained from this plot.

RHEED spot intensity changes during heating and cooling similar to Figs. 4(a) and 4(b). The abrupt changes in intensity due to melting and solidification are clearer than for the 4-ML case. Melting and solidification are observed between the temperature intervals of 600–605 K and 540–547 K,

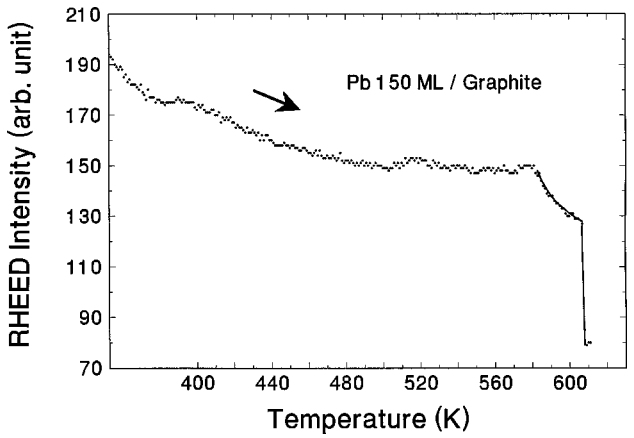

FIG. 8. Temperature-dependent intensity change of the specular beam of 50-ML Pb. An abrupt change in intensity is measured between 605 and 609 K, and a small drop is observed between 580 and 605 K.

respectively. The intensity is seen to drop between 591 and 600 K, but not as abruptly as that observed above 600 K. This intensity change indicates premelting of some crystallites on the surface. From the intensity drop we estimate that nearly 25% of the particles may have premelted. Figure 7(c) is a semilogarithmic plot of RHEED intensity as a function of temperature during heating. A Debye temperature of 91 ± 3 K is obtained from this plot. Similar to the 4-ML case, the graphite spots became more prominent at temperatures between the two steps in the intensity change, where the Pb spots disappear from the RHEED pattern due to Pb melting upon heating, and reappear upon cooling due to solidification.

We have also studied Pb films of thicknesses ~ 70 and ~ 150 ML. The intensity changes with temperature are similar to the 4- and 14-ML cases. Figure 8 shows the intensity change of the 150-ML Pb film. An abrupt change in the intensity is observed between 605 and 609 K. Preceding this, a small drop in intensity is observed between 580 and 605 K. This is attributed to premelting of some Pb crystallites beginning at 580 K. A summary of our results is given in Table III. We conclude that at temperatures above the sudden intensity drop, all of the probed region melted. Some regions of the 70-ML film seem to superheat by as much as 12 ± 2 K, higher than the previous observations for Pb on graphite.

The peak profiles of the specular beam were analyzed and the dependence of the average crystallite size on temperature was estimated. Figures 9(a)–9(c) show the changes in the

TABLE III. Melting, solidification, and Debye temperature of Pb thin films on graphite.

Thickness (ML)	Melting temperature (K)	Solidification temperature (K)	Debye temperature Θ (K)
4	600–(606±2)	530–(535±2)	79±3
14	591–(605±2)	540–(547±2)	91±3
70	598–(613±2)	529–(533±2)	86±3
150	580–(609±2)	523–(532±2)	

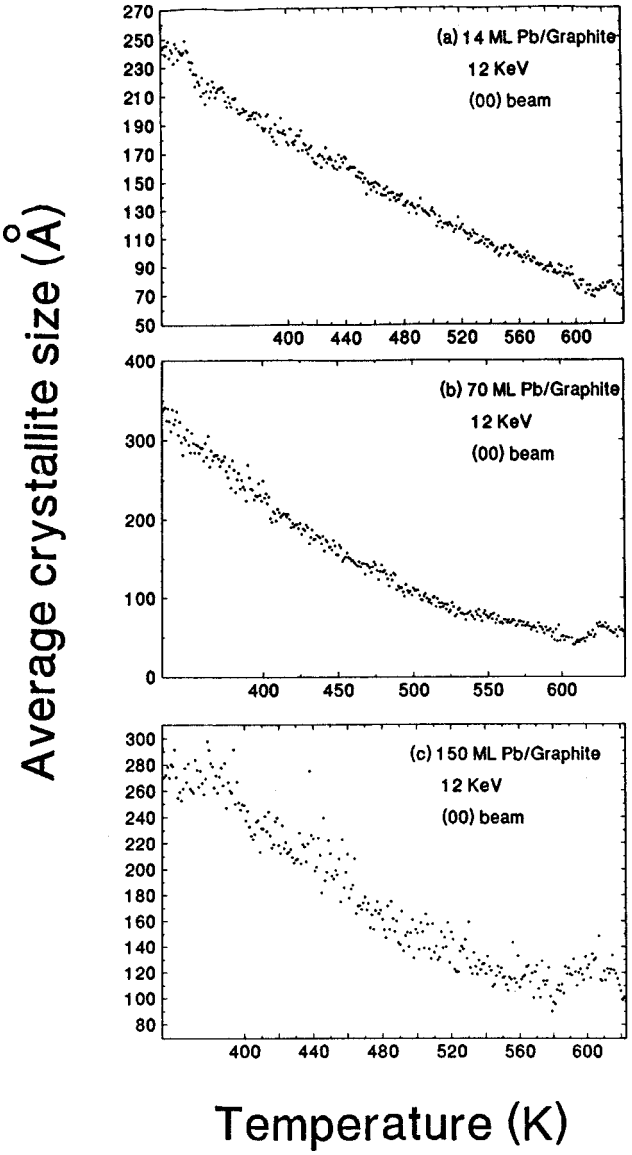

FIG. 9. The changes in the average crystallite size with temperature. (a) 14 ML. (b) 70 ML. (c) 150 ML. The average crystallite size decreases approximately to 100 Å as the temperature reaches T_m.

average crystallite size of the 14-, 70-, and 150-ML thin films of Pb. In each case, the average crystallite size decreases with temperature, approximately to 100±30 Å.

Figures 10(a) and 10(b) are SEM micrographs of ~ 140-ML thick Pb film on graphite. The films were deposited onto the substrate at room temperature in UHV. They were then removed from the UHV system for SEM examinations. Figure 10(a) shows the as-deposited Pb layer without heating after deposition. This clearly shows a large number of 2D thin crystallites (platelets) of Pb. The {111} orientation of these crystallites was determined by RHEED. On some of the 2D layers, small crystallites can be seen, and the growth mode seems to be layer-by-layer growth. Figure 10(b) shows the Pb deposit after treatment by heating to 13 K above the melting point and subsequently cooling to room temperature. Spherical Pb crystallites with an average radius of 0.3 μm are clearly visible.

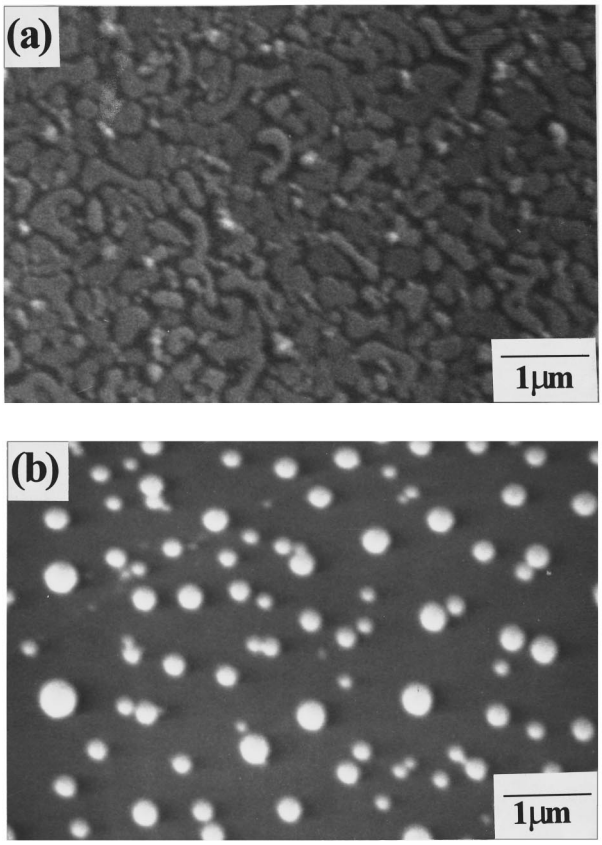

FIG. 10. (a) SEM image taken after depositing ~140 ML of Pb on graphite at room temperature. A large number of 2D layers of Pb can be seen. (b) SEM image after heating the sample up to 13 K above the melting point and subsequently cooling to room temperature. A large number of 3D crystals can be seen.

IV. DISCUSSION

The RHEED observations are in agreement with the previous SEM work of Métois and Heyraud, the Pb layers grow epitaxially on graphite with the Pb(111) surface parallel to the graphite (0002) surface and the [1̄00] direction of the Pb crystal crystallites parallel to the [110] direction of graphite, with the Pb showing {111} texture structure. For low coverage, below 4 ML, both the Pb spots and graphite spots are observed in the RHEED pattern. This indicates the formation of Pb crystallites partially covering the substrate surface. At high coverage, more than ~15 ML, the graphite RHEED spots completely disappear, and are replaced by Pb spots. This indicates full or near full coverage of the graphite surface with Pb{111} layers. Our SEM observations also show the formation of a large number of Pb 2D layers on the graphite substrate. When the sample is heated slightly above the superheating temperature of Pb, the graphite diffraction spots reappear, indicating the exposure of the substrate surface to the electron beam. We assume that the Pb layers condense into liquid droplets after melting, exposing the graphite surface. Subsequently, when the sample temperature is lowered, Pb droplets recrystallize. This occurs at 69 ± 4 K below T_m. We can see these 3D crystals in the SEM micrograph, Fig. 10(b). Previous SEM investigation by Métois and Heyraud showed the formation of spherical Pb particles on graphite after annealing.[1]

Our RHEED intensity measurements indicate that the 4- and the 14-ML films melt completely at 5 ± 2 and 4 ± 2 K above the bulk melting temperature, $T_m = 600.7$ K, respectively. The 70- and the 150-ML films show complete melting at 12 ± 2 and 8 ± 2 K above T_m, respectively. Superheating of Pb crystallites by 3 K was observed by Métois and Heyraud, while superheating of the Pb crystallites by 2 K was observed by Spiller under *in situ* SEM observations.[1,2] Métois *et al.*, observed superheating of Pb crystallites formed by annealing Pb on graphite.[1] Spiller deposited 5 and 50 Å of Pb on to a graphite substrate at 470 K in a low vacuum of 10^{-7} Torr. Spiller found some irregularly shaped particles without sharp corners, in the 50-Å thin film, to superheat by 2 K.[2] The superheating we observe is much larger than that observed in fully annealed Pb layers previously investigated by SEM. This difference can be attributed to the localized heating effects of the electron beam of the SEM and sample preparation. The electron-beam intensity of the SEM is much higher than that of the RHEED beam, thus localized heating due to this beam is significant, being as high as 40 K.[2] Spiller estimates the temperature rise to be 0.5 K on account of the high thermal conductivity of the substrate, neglecting the interface mismatch between the substrate and the film, the presence of domain boundaries, and defects in thin-film layers that may contribute to a decrease in the thermal conductivity. Thus, there may be a difference between the measured and the real values, and that this could explain the discrepancy between our results and those obtained previously. Moreover, in our work we did not pretreat the film as was done by Métois and Heyraud, and Spiller. In their work, the Pb film was melted and recrystallized after Pb was deposited and the film was annealed during the growth.

The Pb atoms deposited at room temperature were seen to grow in 2D layers on the graphite substrate, as can be seen in Fig. 10(a). From intensity profile analysis we conclude that the average size of the crystallite decreases with temperature. Near the melting point, the average crystallite size is 100 ± 30 Å. This indicates that as the temperature is increased, small Pb crystallites form on the graphite surface. Near 570 K, the RHEED pattern of the Pb film shows reflection spots due to Pb{111} crystallites, whereas the measured average size is close to the size at the melting point, $T_m = 600.7$ K. These results indicate that the crystallites with {111} orientation do not change between 570 and 600 K. Therefore, these observations indicate the predominance of small crystallites of Pb with {111} facets near T_m, which undergo the observed superheating.

RHEED intensity measurements indicate that the 4-ML film starts to melt at ~600 K. The 14-, 70-, and the 150-ML films start to melt at 591, 598, and 580 K, respectively. This shows that some of the Pb crystallites undergo premelting as much as 20 ± 2 K below T_m, since the RHEED intensity shows a discontinuous change before the abrupt change shown in Fig. 7(b). This discontinuous change can be due to either premelting or to morphological changes, which can cause the same effect on the intensity. However, as shown in Fig. 9, we did not observe any significantly discontinuous change in the average size of the crystallites near the melting point. Therefore, we conclude that the discontinuous change is due to premelting, not due to morphological changes. This

result is in agreement with results obtained by Spiller and Pavlovska, Faulian, and Bauer.[2,21] In SEM observations, Spiller showed that at 598 K, some liquid particles were present. Pavlovska, Faulian, and Bauer observed a bright ring surrounding the {111} facet above 580 K that shrank and disappeared at T_m.[21] This indicates that premelting starts at the step edge above 580 K. In a theoretical study of step melting on Pb(111),[22] Stewart derived a relation between the surface free-energy density, the size of facets, and the location of edges on the equilibrium crystal shape. These results indicate that an isolated Pb step melts locally above 548 K. The key to step melting is sufficient localization of energy. Stewart's model explained the observed ring in the experiment of Pavlovska, Faulian, and Bauer,[21] e.g., step melting at the edge causes the observed ring at 580 K.

We also observed supercooling of the Pb melt by 69 ± 4 K. This is attributed to a nucleation barrier for solidification that results from the competition between the decrease in free energy upon solidification and the increase in free energy associated with the existence of a solid-liquid interface. The free energy of a solid droplet is related to its radius r. At solid-liquid interfaces, a nucleation barrier for solidification exits for $r<r_0$, where r_0 is some critical radius determined by the surface characteristics of the substrate. The droplets with radii $r<r_0$, supercool. The critical radius estimated for Pb is approximately 40 Å, when the degree of supercooling is 70 K.[20]

V. SUMMARY

We investigated the melting and solidification characteristics of thin films of Pb on graphite using *in situ* RHEED. By measuring the specular beam intensity, an abrupt change in intensity above the bulk melting point of Pb, $T_m = 600.7$ K was clearly observed, which is attributed to superheating of the Pb thin film. By carefully analyzing the RHEED intensity profile, our results also show that the average crystallite size of the deposited Pb layers decrease with temperature. Near T_m, the average crystallite size is found to be 100 ± 30 Å. These results are important for understanding the superheating and melting of Pb thin film on the graphite surface. We observed the melting and solidification of Pb films of thicknesses 4, 14, 70, and 150 ML on graphite. For the investigated film thicknesses, epitaxial growth of Pb at room temperature may occur in a layer-by-layer growth mode. Superheating by $4-(12 \pm 2)$ K above the bulk melting point, and supercooling of the Pb by 69 ± 4 K were observed. Superheating is attributed to the formation of crystallites bounded by the nonmelting Pb{111} surfaces. The surface Debye temperature is calculated from the temperature-dependent RHEED intensity.

ACKNOWLEDGMENT

This work was supported by the U.S. Department of Energy, Division of Materials Science, under Grants Nos. DE-FG05-93ER4 5504 and DE-FG02-97ER45625.

*Electronic address: elsayed-ali@ece.odu.edu

[1] J. Métois and J. C. Heyraud, J. Phys. (France) **50**, 3175 (1989).
[2] G. D. T. Spiller, Philos. Mag. A **46**, 535 (1982).
[3] J. Dáeges and H. Gleiter, Phys. Rev. A **119**, 79 (1986).
[4] J. C. Heyraud and J. J. Métois, Surf. Sci. **128**, 334 (1983).
[5] F. D. Di Tolla, F. Ercolessi, and E. Tosatti, Phys. Rev. Lett. **74**, 3201 (1995).
[6] J. Broughton, Phys. Rev. B **46**, 2523 (1992).
[7] H. E. Elsayed-Ali and J. W. Herman, Rev. Sci. Instrum. **61**, 1636 (1990).
[8] J. W. Herman and H. E. Elsayed-Ali, Phys. Rev. Lett. **69**, 1228 (1992).
[9] J. W. Herman and H. E. Elsayed-Ali, Phys. Rev. B **49**, 4886 (1994).
[10] J. W. Herman, H. E. Elsayed-Ali, and E. A. Murphy, Phys. Rev. Lett. **71**, 400 (1993).
[11] T. J. Wieting and M. Schluter, *Electrons and Phonons in Layered Crystal Structures, Physics and Chemistry of Materials with Layered Structures III* (Reidel, Boston, 1979).
[12] W. N. Reynolds, *Physical Properties of Graphite* (Elsevier, New York, 1968).
[13] H.-J. Guntherodt and R. Wiesendanger, *Scanning Tunneling Microscopy I* (Springer-Verlag, Berlin, 1994), pp. 131–175.
[14] H. X. You, Norman M. N. Brown, and K. F. Al-Assadi, Surf. Sci. **279**, 189 (1992).
[15] J. Valenzuela-Benavides and L. M. de la Garza, Surf. Sci. **330**, 227 (1995).
[16] P. J. Ouseph, T. Poothackanal, and G. Mathew, Surf. Sci. **205**, 65 (1995).
[17] C. Kittel, *Solid State Physics* (Wiley, New York, 1962).
[18] M. A. Van Hove and C. M. Chen, *Low Energy Electron Diffraction* (Springer-Velag, Berlin, 1989).
[19] M. Jalochowski and E. Bauer, Phys. Rev. B **37**, 8622 (1988); **38**, 5272 (1988).
[20] J. W. Herman and H. E. Elsayed-Ali (unpublished).
[21] A. Pavlovska, K. Faulian, and E. Bauer, Surf. Sci. **221**, 233 (1989).
[22] J. Stewart, Phys. Rev. B **49**, 13 826 (1994).